Polarization-resolved second harmonic generation microscopy of chiral G-shaped metamaterials

Evgeniy A. Mamonov,[1,*] Anton I. Maydykovskiy,[1] Irina A. Kolmychek,[1] Sergey A. Magnitskiy,[1,2] and Tatiana V. Murzina[1]
[1]*Department of Physics, M.V. Lomonosov Moscow State University, Leninskie Gory, Moscow 119991, Russia*
[2]*International Laser Center, M.V. Lomonosov Moscow State University, Leninskie Gory, Moscow 119991, Russia*
(Received 9 December 2016; revised manuscript received 10 July 2017; published 7 August 2017)

Chiral planar metamaterials are known for their possibility to show strong nonlinear optical effects such as second harmonic generation (SHG) circular dichroism or asymmetric SHG. The underlying mechanisms are commonly discussed in terms of local field effects and formation of localized SHG sources (so called "hotspots") that are sensitive to the shape and size of meta-atoms. Nevertheless, a full characterization of the polarization state of the nonlinear optical radiation from the hotspots has not been performed until now. Here we present the results of the polarization-resolved second harmonic generation microscopy studies of planar chiral G-shaped metamaterials. We demonstrate that the SHG radiation coming from the hotspots that are localized within a single meta-atom is partially polarized; moreover, the SHG polarization state reveals the chirality of the structure. The observed effects are attributed to the induced plasmonic current oscillations at the fundamental frequency along with the local field distribution.

DOI: 10.1103/PhysRevB.96.075408

Metamaterials have been experiencing a continuous growth of interest over the last decade due to their remarkable optical properties [1–3]. It was demonstrated that metamaterials reveal new functional capabilities based on their tunable, switchable, and nonlinear properties that provide perspective for applications in functional devices [4,5]. The optical response of metamaterials originates from a specific design of a single nanoelement (meta-atom) and an array as a whole and is governed by the spatial distribution of the local optical field and by its resonant behavior [6,7]. That is why the studies of the field distribution within a single meta-atom are strongly desired for the understanding of the physical mechanisms underlying the interaction of light with metamaterials [8,9].

Among various optical techniques, second harmonic generation (SHG) microscopy is very attractive here as it can reveal precisely the field localization on the submicron scale [10,11]. SHG microscopy was successfully used for the visualization of the local field distribution within chiral meta-atoms of 1 μm in size that form a planar metasurface, and it showed a strong SHG localization ("SHG hotspots") caused by the excitation of localized surface plasmons [12,13]. At the same time, coherence and polarization state of the SHG radiation from the hotspots have not been studied in detail, although they contain important information about the nature of the field localization within meta-atoms. These SHG parameters can be studied using the polarization-resolved SHG microscopy. This technique is known for its high contrast and signal-to-noise ratio of images as compared to ordinary SHG microscopy [14,15], as well as providing additional information about structural properties of the samples [16–18]. It was demonstrated that application of this technique to microstructures allows one to separate the SHG contributions from different parts of the structure [19].

In this article, we study experimentally parameters of the SHG from the hotspots in G-shaped chiral nanostructures. Moreover, we demonstrate that the polarization of the SHG from the hotspots is partially polarized and the corresponding polarization state is sensitive to the G-shaped structures' handedness: it governs the SHG polarization plane rotation direction and the sign of the ellipticity.

The studied planar *chiral* metasurfaces consist of periodic arrays of gold G-shaped nanostructures (meta-atoms) deposited on a Si(001) substrate covered by a 200-nm-thick SiO_2 dielectric layer. The thickness of the meta-atoms is 30 nm, the lateral size of the elements is 1 μm, and the distance between them in an ensemble is 200 nm; other sizes of the structure are shown in Fig. 1(b). The samples were made by the electron-beam lithography method; the details can be found in [20]. Each sample contains 2000 × 2000 G-shaped nanostructures oriented in a similar way on the substrate.

The experimental setup [Fig. 1(a)] was based on a femtosecond Ti:sapphire laser system operating at the wavelength of 800 nm. Laser radiation with the repetition rate of 80 MHz and pulse duration of 60 fs passed through a red filter (Schott, RG 695), a half-wave plate for the control of the polarization of the fundamental beam and through a long-pass dichroic mirror. The fundamental beam was focused onto the sample by the objective Leica PL FLUOTAR L 63× with the numerical aperture of 0.7 providing the spatial resolution of 460 nm at the second harmonic (SH) wavelength. The SH radiation generated in the reflection was collected by the same objective; the details about the laser and the objective can be found in the work [21]. The sample was mounted on a home-made three-dimensional (3D) translation stage, the translation in the lateral plane was performed with an accuracy of approximately 10 nm. The nonlinear optical (NLO) signal generated by the sample was reflected from the dichroic mirror and passed through a colored filter (center wavelength 400 nm, FWHM 60 nm) to cut most of the part of the two-photon luminescence (TPL). The intensity spectrum of the registered nonlinear optical signal containing SHG and TPL is shown in Fig. 1(c), the averaged contribution of the TPL being less than 40% from the total registered intensity. Then it passed through quarter-wave and half-wave plates, was divided into two beams with orthogonal polarizations by a polarizing beam splitter (PBS) and detected by the two photomultipliers (PMTs) operating in the photon counting mode. This experimental setup allowed

*mamonov@shg.ru

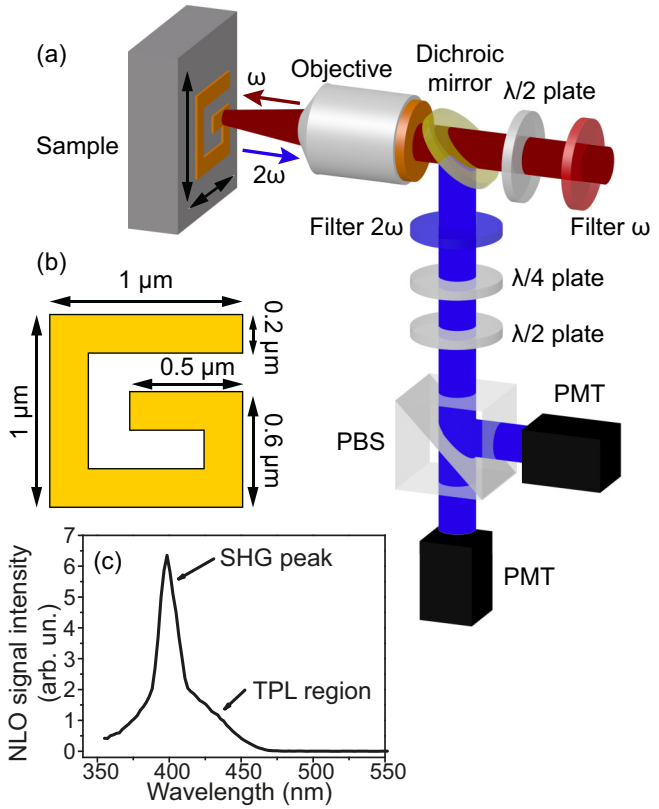

FIG. 1. (a) Scheme of the experimental setup, (b) scheme of a single structure, and (c) spectrum of the collected nonlinear optical signal.

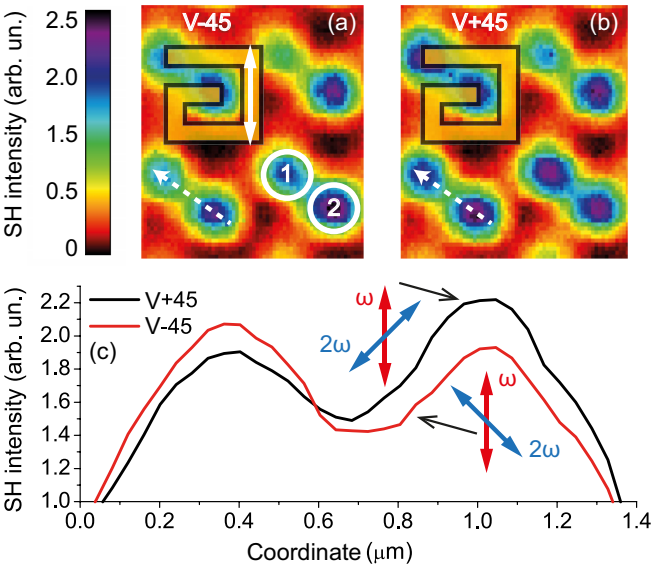

FIG. 2. Spatial distributions of the SHG intensity for the periodic array of G-shaped structures. Polarization of the fundamental beam is vertical, polarization of the SH beam is rotated by (a) −45° or (b) +45° in relation to the fundamental beam polarization. (c) Cross sections of the SHG patterns shown in panels (a) and (b), red and blue arrows show schematically the orientation of the polarization plane of the fundamental and SH radiation, respectively, in the two hotspots.

us to measure simultaneously the Stokes parameter S_0 and one of the three other parameters (S_1,S_2, and S_3) depending on the orientation of the wave plates [22]. The instrumental Mueller matrix was measured [23] and the corresponding normalization of the registered SHG signal was performed. In order to study the local SHG polarization state, the Stokes parameters were calculated and spatial patterns of the SHG polarization state were obtained.

In order to characterize the SHG polarization state generated by the metasurface the NLO intensity distribution was measured for six different SHG polarizations: horizontal I_H, vertical I_V, $I_{\pm 45}$, rotated to ±45 degrees relative to the fundamental beam polarization, and left-circular polarization (I_{LCP}) and right-circular polarization (I_{RCP}) circular polarizations. This allowed us to estimate all Stokes parameters for SHG $S_0 = I_H + I_V$, $S_1 = I_H - I_V$, $S_2 = I_{45^o} - I_{-45^o}$, and $S_3 = I_{\mathrm{RCP}} - I_{\mathrm{LCP}}$ because it was checked that the TPL was unpolarized. The ellipticity angle $\varepsilon_\theta = \frac{1}{2}\arctan\left(\frac{S_3}{\sqrt{S_1^2+S_2^2}}\right)$ and polarization ellipse orientation angle $\phi = \frac{1}{2}\arctan\left(\frac{S2}{S1}\right)$ were also obtained from the measured data. To obtain the values of the polarization parameters in the SHG hotspots, spatial distributions of the parameters were averaged over the hotspot area that was about 450 nm, as can be seen in Fig. 2. The degree of polarization (DOP), $\frac{\sqrt{S_1^2+S_2^2+S_3^2}}{S_0}$, for all studied experimental geometries was about 55% due to hyper Rayleigh scattering [24]. The DOP was estimated from the obtained data after extracting the contribution of the unpolarized TPL.

Figures 2(a) and 2(b) show the spatial distribution of the SHG intensity in mirror-G-shaped nanostructures excited by the vertically polarized fundamental beam denoted by white arrow. The ±45° polarization of the SHG radiation (i.e., linear polarization of the SH wave rotated by 45° clockwise or counterclockwise in relation to the fundamental beam polarization, respectively) was detected and used for the estimation of the Stokes parameter S_2. It can be seen that there are two areas within a single meta-atom with high SHG intensity, i.e., hotspots, denoted by the numbers 1 (upper) and 2 (lower) in Fig. 2(a), their spatial distribution corresponds to the results reported in [13]. Moreover, the SHG intensities in these hotspots are different, that is visualized by the cross section [Fig. 2(c)] of the intensity pattern intersecting a single nanostructure along the dashed line shown in Figs. 2(a) and 2(b). The SHG intensity in hotspot 1 is larger for +45° SHG polarization as compared to that obtained for −45°, while for hotspot 2 the dependencies are reversed. This means that the S_2 parameter in the two hotspots is of a different sign.

The estimated parameter S_1 turned out to be of a constant (positive) sign all over the structure. Along with the alternating sign of the Stokes parameter S_2 this means that the linearly polarized part of the SHG radiation generated by hotspots 1 and 2 is rotated in different directions relatively to the fundamental beam polarization. The estimated values of the rotation angle are $\phi_1 = 27^\circ \pm 2^\circ$ and $\phi_2 = -32^\circ \pm 2^\circ$ [Fig. 3(a)] for the upper and lower hotspots, respectively. Importantly, the spatial distribution of the SHG polarization state for another enantiomorph of the G-shaped metasurface [Fig. 3(b)] is mirror symmetric to that shown in Fig. 2(a), with the rotation angles of the polarization ellipse being $\phi_1 = -24^\circ \pm 2^\circ$ and $\phi_2 = -28^\circ \pm 2^\circ$. According to our estimations, the SHG ellipticity

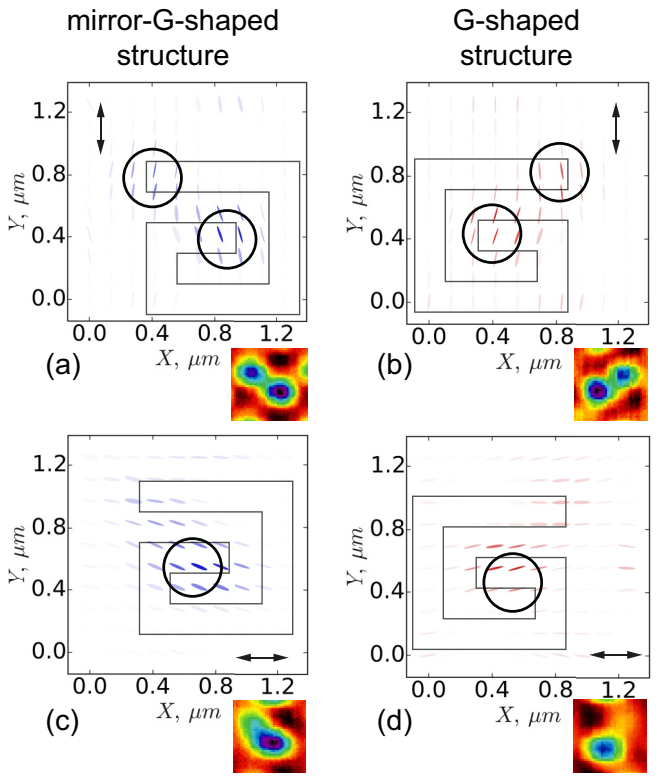

FIG. 3. Distributions of SHG polarization state (ellipses) within a single structure calculated using the experimental dependencies of the Stokes parameters for mirror-G-shaped (a) and (c) and G-shaped samples (b) and (d). The fundamental beam polarization is shown by arrows. The transparency of the ellipses denotes the SHG intensity of the given point. Ellipse color denotes the sign of the SHG ellipticity, red for "+" and blue for "−". Hotspot areas are denoted by black circles according to the work [25]. Colored insets show the distribution of the SHG intensity under the corresponding experimental conditions.

angle ε_θ is small, and its averaged value is $5^\circ \pm 1^\circ$ for the G-shaped structure and $-4.5^\circ \pm 0.8^\circ$ for the mirror-G-shaped structure. Again, different signs of ε_θ for G and mirror-G structures is an indication that the circularly polarized part of the second harmonic radiation for the two enantiomorphs is of different handedness and thus reveals the chirality of the nonlinear optical interaction with such a metasurface.

In the case of the horizontally polarized fundamental beam there is only one strong hotspot in the structure, which is in agreement with the previous work [13]. SH radiation from this hotspot is also found to be polarized, as in the case of the vertically polarized fundamental beam, and its polarization plane is rotated to $\phi = 21^\circ \pm 1^\circ$ in relation to the fundamental beam polarization plane. The mirror-G-shaped structure demonstrates similar behavior with the angle of the SH polarization plane rotation of $\phi = -21^\circ \pm 1^\circ$. These results are summarized in Fig. 3, which shows the spatial distribution of the SHG polarization state estimated from the obtained experimental data.

It is also worth noting that the handedness of the circularly polarized component of the SHG radiation is also different, the ellipticity angles being $6^\circ \pm 1^\circ$ and $-5^\circ \pm 1^\circ$ for G-shaped and mirror-G-shaped samples, respectively. The similar effect

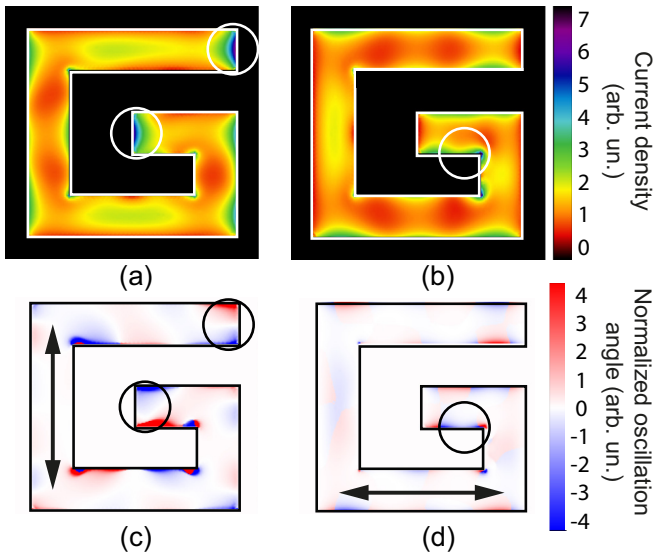

FIG. 4. Spatial distributions of (a) and (b) current density and (c) and (d) tilt angle of the direction of the current density oscillations at the fundamental wavelength multiplied by the squared current amplitude within the G-shaped nanostructure for (a) and (c) vertical and (b) and (d) horizontal polarization of the fundamental beam, the hotspot areas are shown schematically by black circles. Vertical and horizontal polarization planes of the fundamental wave are shown by black arrows. The angle is measured out from the fundamental radiation polarization plane.

of the different efficiency of circularly polarized SHG in enantiomorphs (inverse SHG-circular dichroism (CD) effect) has also been observed earlier in the arrays of G-shaped nanostructures [26] in the far field, where parameters of the effect can be significantly influenced by the sample's azimuthal position [27].

In order to analyze the optical response of the structure, we perform the simulations of the induced current density and the local electric field at the fundamental wavelength, as these quantities influence significantly the parameters of SHG [28]. The simulations by means of the finite element method are made using the CST MICROWAVE STUDIO software [29–31] for a single G-shaped nanoelement located in the array with the geometrical and structural parameters identical to the real ones, when using the Gaussian shape of the fundamental radiation source. The distribution of all the components of the current density at the fundamental wavelength at a distance of 4 nm below the Au-air interface inside the structure are calculated. Then the direction of oscillations (the angle between the current oscillation direction and of the polarization plane of the fundamental radiation) of the current density within a single G-shaped structure is obtained.

As the local plasmon excitation leads to a strong inhomogeneity of the local current density and thus to an essential localization of the SHG sources, so the directions of the current oscillations at the fundamental frequency should be averaged with the weights equal to the squared local current densities (Fig. 4), as the SHG is a second-order process [28].

The corresponding results for the G-shaped sample induced by the vertically and horizontally polarized fundamental beam are shown in Fig. 4. It can be seen from Figs. 4(a) and 4(b) that

the spatial modulation of the current density at the fundamental wavelength is less pronounced as compared to that of the SHG intensity measured in the experiment. At the same time, a good correlation between the experiment and the model calculations are attained when we take into account that the SHG intensity should be proportional to the fourth power of the local current density [28,32]. These hotspot areas can be visualized using a higher intensity of the fundamental beam that can cause damage to the nanostructure [25]. Averaging over the hotspot areas shows that in the first case, as the two hotspots are formed, the effective oscillations of the current density (as well as those of the local electric field) in the hotspots' areas are turned in opposite directions. In the case of the horizontal linear polarization of the fundamental beam (one hotspot), the current density and the local electric field oscillation plane [Fig. 4(d)] are turned in the same direction as for the lower hotspot shown in Fig. 4(c). It is obvious that maps of the averaged directions of the current density oscillations demonstrate qualitatively the same peculiarities as the distribution of the SHG polarization ellipses orientations.

Analogous simulations of the current density on the second harmonic frequency were performed, but did not reveal any pronounced dependencies; the average angle of the current density oscillation direction is close to zero in hotspot areas. Thus the observed SHG polarization parameters are governed by the optical response of the nanostructures under study at the fundamental frequency.

In conclusion, the polarization-resolved second harmonic generation microscopy technique is first applied to study the nonlinear optical response of chiral nanostructures. It is found that polarization of the SHG radiation from the hotspots in G-shaped metamaterials is mostly linear and reveals the chirality of the structure; different rotation direction of the SH polarization plane in the hotspots and different handedness of circularly polarized SHG components are observed for the mirror-symmetric G-shaped enantiomorphs. Simulations of the induced current density spatial distribution at the fundamental wavelength in the G-shaped metasurfaces show that the SHG polarization plane in hotspots is rotated in the same direction as the oscillations of induced plasmonic currents in the structure. The results may be used to further describe the nonlinear optical response of the metasurfaces.

We are thankful to V. K. Valev for fruitful discussions. The financial support from Russian Science Foundation (RSF) Grant No. 16-42-02024 is greatly acknowledged.

[1] W. Cai and V. Shalaev, *Optical Metamaterials* (Springer-Verlag, New York, 2010).
[2] Y. Liu and X. Zhang, Chem. Soc. Rev. **40**, 2494 (2011).
[3] M. Lapine, I. V. Shadrivov, and Y. S. Kivshar, Rev. Mod. Phys. **86**, 1093 (2014).
[4] J. Butet, P.-F. Brevet, and O. J. F. Martin, ACS Nano **9**, 10545 (2015).
[5] M. Kauranen and A. V. Zayats, Nat. Photonics **6**, 737 (2012).
[6] F. von Cube, S. Irsen, R. Diehl, J. Niegemann, K. Busch, and S. Linden, Nano Lett. **13**, 703 (2013).
[7] N. I. Zheludev and Y. S. Kivshar, Nat. Mater. **11**, 917 (2012).
[8] P. C. Wu, W.-L. Hsu, W. T. Chen, Y.-W. Huang, C. Y. Liao, A. Q. Liu, N. I. Zheludev, G. Sun, and D. P. Tsai, Sci. Rep. **5**, 9726 (2015).
[9] H. Husu, B. K. Canfield, J. Laukkanen, B. Bai, M. Kuittinen, J. Turunen, and M. Kauranen, Appl. Phys. Lett. **93**, 183115 (2008).
[10] C. K. Chen, T. F. Heinz, D. Ricard, and Y. R. Shen, Phys. Rev. B **27**, 1965 (1983).
[11] H. Shen, N. Nguyen, D. Gachet, V. Maillard, T. Toury, and S. Brasselet, Opt. Express **21**, 12318 (2013).
[12] V. K. Valev, N. Smisdom, A. V. Silhanek, B. D. Clercq, W. Gillijns, M. Ameloot, V. V. Moshchalkov, and T. Verbiest, Nano Lett. **9**, 3945 (2009).
[13] V. K. Valev, A. V. Silhanek, N. Smisdom, B. D. Clercq, W. Gillijns, O. A. Aktsipetrov, M. Ameloot, V. V. Moshchalkov, and T. Verbiest, Opt. Express **18**, 8286 (2010).
[14] J. M. Bueno and M. C. W. Campbell, Opt. Lett. **27**, 830 (2002).
[15] J. Bueno, C. Cookson, M. Kisilak, and M. Campbell, J. Microsc. **235**, 84 (2009).
[16] S. Brasselet, Adv. Opt. Photonics **3**, 205 (2011).
[17] M. A. van der Veen, F. Vermoortele, D. E. D. Vos, and T. Verbiest, Anal. Chem. **84**, 6378 (2012).
[18] C. Awada, C. Jonin, F. Kessi, P. Adam, S. Kostcheev, R. Bachelot, P. Royer, M. Samah, I. Russier-Antoine, E. Benichou, G. Bachelier, and P. Brevet, Opt. Mater. **33**, 1440 (2011).
[19] S. I. Bozhevolnyi, A. Maidykovski, B. Vohnsen, and V. Zwiller, J. Appl. Phys. **90**, 6357 (2001).
[20] V. K. Valev, X. Zheng, C. Biris, A. Silhanek, V. Volskiy, B. D. Clercq, O. A. Aktsipetrov, M. Ameloot, N. C. Panoiu, G. A. E. Vandenbosch, and V. V. Moshchalkov, Opt. Mater. Express **1**, 36 (2011).
[21] A. M. Dubrovkin, Y. Jung, V. M. Kozenkov, S. A. Magnitskii, and N. M. Nagorskiy, Laser Phys. Lett. **4**, 275 (2007).
[22] J. T. Madden, V. J. Hall, and G. J. Simpson, Analyst **136**, 652 (2011).
[23] N. Mazumder, J. Qiu, M. R. Foreman, C. M. Romero, C.-W. Hu, H.-R. Tsai, P. Török, and F.-J. Kao, Opt. Express **20**, 14090 (2012).
[24] E. A. Mamonov, T. V. Murzina, I. A. Kolmychek, A. I. Maydykovsky, V. K. Valev, A. V. Silhanek, E. Ponizovskaya, A. Bratkovsky, T. Verbiest, V. V. Moshchalkov, and O. A. Aktsipetrov, Opt. Lett. **36**, 3681 (2011).
[25] V. K. Valev, Langmuir **28**, 15454 (2012).
[26] E. Mamonov, T. Murzina, I. Kolmychek, A. Maydykovsky, V. Valev, A. Silhanek, T. Verbiest, V. Moshchalkov, and O. Aktsipetrov, Opt. Express **20**, 8518 (2012).
[27] E. Mamonov, I. Kolmychek, T. Murzina, A. Maydykovsky, O. Aktsipetrov, V. Valev, T. Verbiest, A. Silhanek, and V. Moshchalkov, J. Phys.: Conf. Ser. **352**, 012029 (2012).
[28] N. Bloembergen, *Nonlinear Optics* (World Scientific, Singapore, 1996).
[29] E. Tatartschuk, E. Shamonina, and L. Solymar, Opt. Express **17**, 8447 (2009).
[30] Y. Liu, S. Palomba, Y. Park, T. Zentgraf, X. Yin, and X. Zhang, Nano Lett. **12**, 4853 (2012).
[31] P. Ghenuche, S. Cherukulappurath, T. H. Taminiau, N. F. van Hulst, and R. Quidant, Phys. Rev. Lett. **101**, 116805 (2008).
[32] O. A. Aktsipetrov, I. M. Baranova, S. S. Elovikov, P. V. Elyutin, D. A. Esikov, A. A. Nikulin, and N. N. Fominykh, JETP Lett. **41**, 615 (1985).